

**MEMORANDUM
RESEARCH DEPARTMENT**



To: HR, HO, HMD, RD staff and consultants

Date: 24 July 2002

From: Saleh Abdalla, Jean Bidlot

Ref.: R60.9/SA/0273

Subject: **Wind Gustiness and Air Density Effects and Other Key Changes to Wave Model in CY25R1**

Abstract:

The key features of the wave model contribution to CY25R1 are classified under three categories: wind gustiness and variable air density, removal of spurious effects in the determination of the Charnock parameter, and data analysis. Theoretical and numerical studies have showed that wind gustiness has an important role in enhancing wave growth under unstable conditions. Although the role of air density is less pronounced, it should not be ignored. The impact of both processes on wave growth was implemented in CY25R1. The interface between the atmospheric model and the wave model was generalised to accommodate any additional fields in either direction with minimum effort. Initial wave conditions are introduced at sea points emerged after the sea ice retreat. This eliminates the spikes in the Charnock parameter field at those points. Blacklisting was introduced for the wave model using a separate list from that used by the atmospheric model. Other numerical and technical issues were introduced to enhance the model performance and to keep the Charnock parameter values within a more realistic range.

1. Wind Gustiness and Air Density:

Introduction:

Wind-wave modelling has reached a rather satisfactory level for practical applications with the development of the third generation wave models (e.g., Komen *et al.*, 1994). At the same time the progressive improvement in meteorological modelling, and in particular in the description of the surface wind fields, has led to the gradual decrease in errors experienced in the last decade (see, e.g., Jacob *et al.*, 2000, and Bidlot *et al.*, 2000). Although the current level of accuracy in wave modelling is quite satisfactory for a wide range of practical applications, it still needs some enhancement. Part of this can be achieved by including the impact of various phenomena not modelled explicitly. Wind gustiness and actual air density are two important examples.

The intrinsic variability of the atmosphere, especially at small scales, are not sufficiently represented in the present meteorological models (see Simmons, 1991, and

Cavaleri *et al.*, 1997). The implications of the sub-synoptic variability, which we will refer to as gustiness, for the evaluation of wind waves in the oceans was addressed by a number of researchers (e.g. Janssen, 1986, Cavaleri and Burgers, 1992; Komen *et al.*, 1994; Bauer and Weisse, 2000; and Abdalla and Cavaleri, 2002).

Wave models usually assume a constant air density ($\rho_a \approx 1.225 \text{ kg/m}^3$) throughout. Actual air density is neither homogeneous nor steady. Variations in air density can reach up to $\pm 20\%$ compared to the traditional value usually used in typical wave models. This implies the need for a more realistic representation of the air density in wave models.

Wind Input Source Term:

From the wave modelling point of view, both wind gustiness and air density affect wave generation through the wind input source term that can be written generically as (e.g., Komen *et al.*, 1994):

$$\frac{\partial F}{\partial t} = \gamma F \quad \text{with} \quad \gamma = \gamma\left(\frac{\rho_{air}}{\rho_{water}}, U\right)$$

where, F is the energy density of a wave component, t is the time, $\rho_{air} / \rho_{water}$ is the air-water density ratio (which is usually assumed constant in wave models), and U is the wind (or the friction) velocity component along wave propagation direction. Usually mean wind (friction) velocity is used. This implies an ignorance of the impact of sub-grid, and even larger-scale, wind variability on wave generation.

Wind Gustiness:

There is a fair amount of information on the variability of the atmosphere at the different scales. A general description of the characteristics of surface winds on the oceans can be found, e.g., in Freilich and Chelton (1986) and Tournadre and Blanquet (1994). Several dedicated experiments were conducted to study the small-scale characteristics, e.g. HEXOS (Smith *et al.*, 1990). Notwithstanding this wealth of information, most of it has not yet found its way to wave modelling due to several reasons. Mainly, the level of gustiness present in the atmosphere is partially filtered in the available meteorological models as a result of the artificial numerical diffusion introduced in those models ensure their numerical stability (see Simmons, 1991).

There is ample evidence (e.g. Munn, 1966, and Smith *et al.*, 1990) that the fluctuations of wind speed and direction around an average value are well represented by a Gaussian distribution. There are two main approaches to include the wind speed variability in wave modelling. The first approach is the use of the Monte-Carlo simulation technique by superimposing random variability over the model (mean) wind speeds as was done by Cavaleri and Burgers (1992) and Abdalla and Cavaleri (2002). This approach provides instantaneous impact that may not represent the actual one. For the mean impact, one needs

to carry out (at least) several tens of realisations and average their impact. This is not a practical solution for operational systems.

The other alternative is to replace the traditional input source term in the model by an enhanced form that includes the mean impact of gustiness as was done by Janssen (1986) and by Miles and Ierley (1998). Although it only gives the mean impact of the gustiness, this approach is rather convenient for operational applications.

The current set-up of the coupled ECMWF operational system passes the wind fields from the atmospheric model to the wave model at each time step (15 minutes). With this set-up, one can assume that the wind speed variations with scales much larger than both the spatial resolution and the time step are already resolved (apart from the impact of the added numerical diffusion). Therefore, we need to include the impact of the variability at scales comparable to or lower than the model resolution. To achieve this, an enhanced input source term with the mean impact of gustiness can be estimated as:

$$\bar{\gamma}(u_*) = \int_{u_*=-\infty}^{\infty} \frac{1}{\sigma_* \sqrt{2\pi}} \exp\left(-\frac{(u_* - \bar{u}_*)^2}{2\sigma_*^2}\right) \gamma(u_*) du_*$$

where u_* represents the instantaneous (unresolved) wind friction velocity, σ_* is the standard deviation of the friction velocity and the over-bared quantity represents the mean value of the quantity over the whole grid-box/time-step. Note that \bar{u}_* is the (gust-free) value obtained from the atmospheric model. The integral above can be approximated using the Gauss-Hermite quadrature as:

$$\bar{\gamma}(u_*) \cong 0.5 \left[\gamma(\bar{u}_* - \sigma_*) + \gamma(\bar{u}_* + \sigma_*) \right]$$

The magnitude of variability can be represented by the standard deviation of the wind speed. To estimate the standard deviation value, one can use the empirical expression proposed by Panofsky *et al.* (1977) which can be written as:

$$\frac{\sigma_{10}}{u_*} = \left[b + 0.5 \left(\frac{z_i}{-L} \right) \right]^{1/3}$$

where σ_{10} is the standard deviation of the 10-m wind speed, z_i is the height of the lowest inversion, L is the Monin-Obukhov length, and b is a constant representing the background gustiness level that exists all the times irrespective of the stability conditions. The quantity $(z_i / -L)$, which is a measure for the atmospheric stability, is computed by the atmospheric model. The impact of the background level of gustiness is/should be already included implicitly in the parameterisations of the atmospheric model as well as in the wave model. Therefore, the constant b value is used as 0.

The WAM model is formulated in terms of the wind friction velocity, u_* , rather than the surface wind velocity, U_{10} . On the other hand, the empirical evidences support the

Gaussian distribution of U_{10} . The relation between U_{10} and u^* is non-linear and depends on the sea-state. Therefore, the relation between σ_{10} and σ^* is not readily available. A transformation between σ_{10} and σ^* is done using:

$$\sigma^* \cong \left[1.0 + 0.5 (U_{10} / C_D) 0.08 \times 10^{-3} \right] \sigma_{10}$$

$$\text{where; } C_D \cong 0.8 \times 10^{-3} + 0.08 \times 10^{-3} U_{10}$$

Air Density:

The air density depends on the air temperature, pressure and humidity. Therefore, the air density field is neither steady nor homogeneous. Abdalla and Cavaleri (2002) show that the overall mean impact of considering the actual air density (as estimated from the atmospheric conditions) on wave modelling results is almost negligible. However, for specific events the impact can be rather significant.

Based on basic thermodynamic concepts, it is possible to compute the air density using the following formula:

$$\rho_{air} = \frac{P}{R T_v}$$

where P is the atmospheric pressure, R is a constant ($\approx 287.04 \text{ J}\cdot\text{kg}^{-1}\cdot\text{K}^{-1}$) defined as $R = R^* / m_a$, with R^* is the universal gas constant ($\approx 8314.36 \text{ J}\cdot\text{kmol}^{-1}\cdot\text{K}^{-1}$) and m_a is the molecular weight of the dry air ($\approx 28.966 \text{ kg}\cdot\text{kmol}^{-1}$) and T_v is the virtual temperature. The virtual temperature can be related to the actual air temperature, T , and the specific humidity, q , by: $T_v \approx (1 + 0.6078 q) T$. The pressure (mean sea-level pressure, MSL, is used), temperature (skin temperature is used) and specific humidity (humidity at 2-m height is used) are all standard products of the meteorological model.

Results:

Before the current implementation of wind gustiness and air density, the two-way coupling between the atmospheric model and the wave model implied the transfer of the wind fields, U_{10} and V_{10} , in the atmosphere-wave direction and the Charnock parameter field, α , in the wave-atmosphere direction. The current implementation implies more data traffic in the atmosphere-wave direction with four extra fields; namely: mean sea-level pressure (P), humidity at 2-m (q), skin temperature (T) and the stability parameter z/L as shown schematically in Figure 1.

Several experiments were carried out to test this implementation using low-resolution model (T159). The positive impact encouraged the application with the current T511/L60 model resolution. The spatial resolution of the atmospheric model is about 40 km while that of the wave model is 55 km. The integration time step is 15 minutes. There is a two-way

coupling between the atmospheric and the wave models at each time step. This set-up was run for the period 22 November – 14 December 2000. The wave scores (anomaly correlation and standard deviation of error) of the significant wave height compared to those of the control run are shown in Figure 2 for the 23 cases. Although the Northern Hemisphere (NH) scores are rather neutral for the first 7 days, remarkable positive impact can be seen for the Southern Hemisphere (SH). The impact was further verified by computing the difference statistics between the model forecast significant wave heights and the ERS-2 radar altimeter significant wave height measurements as shown in Figure 3. The current implementation causes minor reduction in the root mean square differences (RMSE) and enhances the correlation between the forecast and the altimeter measurements. Furthermore, the negative bias was remarkably reduced in the NH. This is a direct result of the fact that under active areas (winter in the NH) the gustiness increases the wave heights.

Table 1 shows the individual impacts on the wave height contributed by the wind gustiness and the air density separately based on the period 22 – 29 Nov. 2000 (8 days). Similarly, Table 2 shows the impacts on the geopotential at 500hPa.

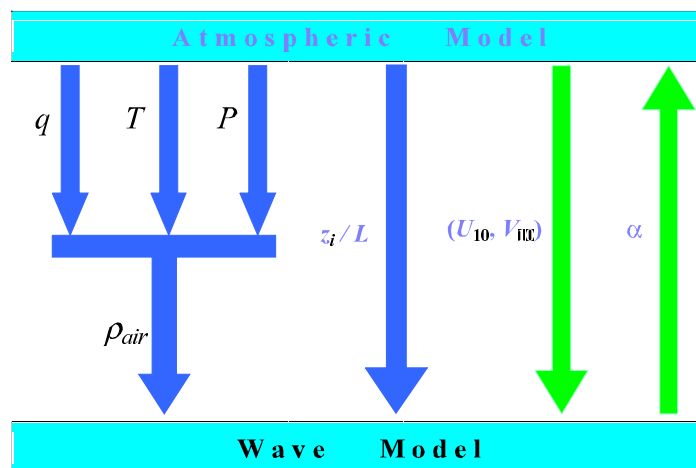


Figure 1: Data traffic across the atmospheric/wave model interface since CY25R1. (Green is the already existing traffic before CY25R1, blue is the additional traffic.)

Table 1: Gustiness and air density impacts on significant wave height (22-29 Nov. 2000).

<i>SWH</i> , 8 cases	Gustiness	Air Density	Both
NH	↔	–	–
Tropics	+	–	↔
SH	+	+	+

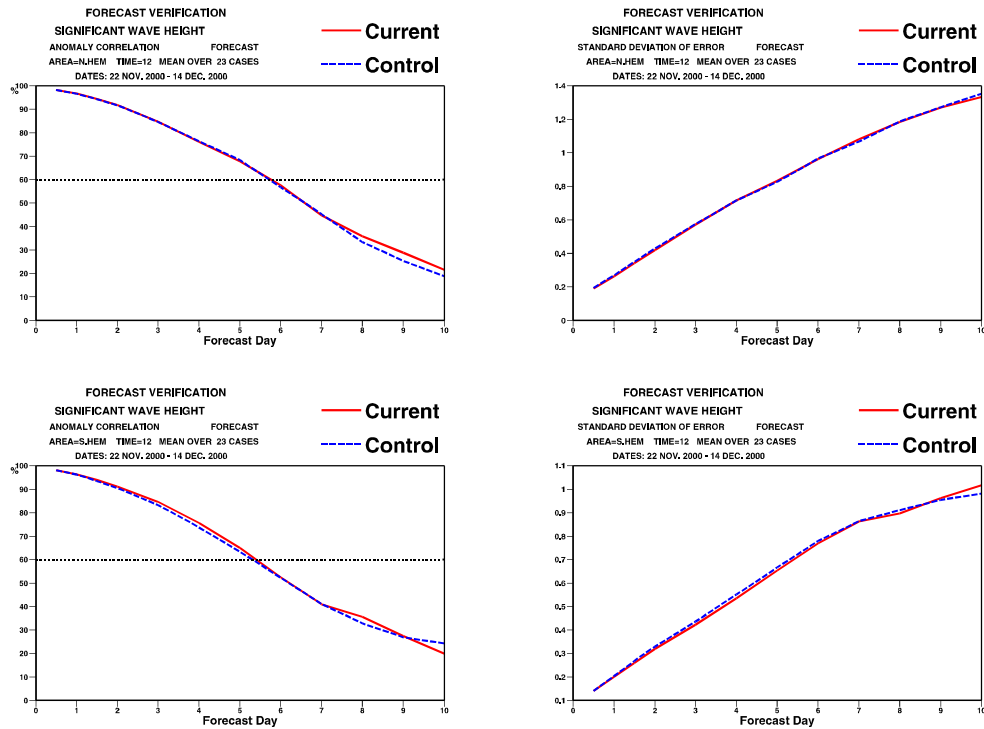


Figure 2: Significant wave height scores (anomaly correlation and standard deviation of error) for 22 Nov. - 14 Dec. 2000 for NH (upper two panels) and SH (lower panels).

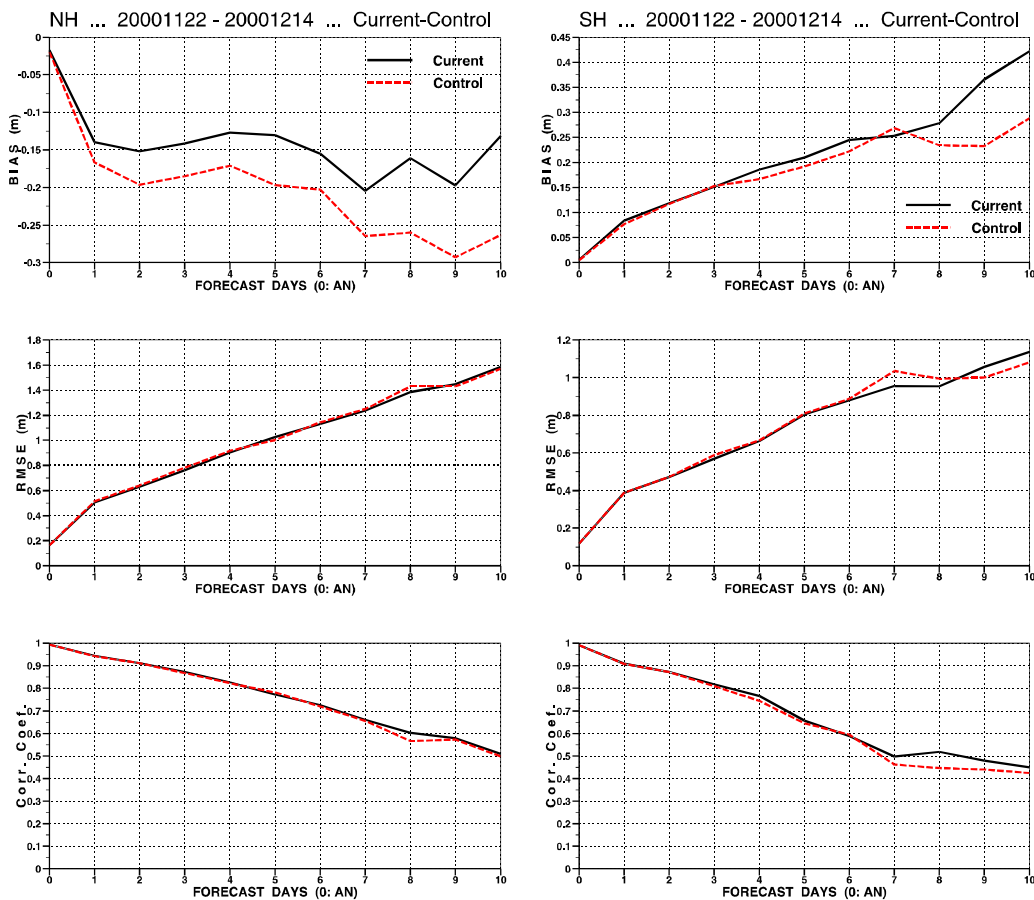


Figure 3: Comparison between model forecast and ERS-2 radar altimeter significant wave heights during 22 Nov. - 14 Dec. 2000 for NH (left panels) and SH (right panels).

Table 2: Gustiness and air density impacts on geopotential at 500 hPa (22-29 Nov. 2000).

Z,	8 cases	Gustiness	Air Density	Both
	NH	-	-	-
	Tropics	+	+	+
	SH	↔	+	+

Conclusions:

The impact of the wind gustiness and a realistic estimation of the air density were introduced into the ECMWF system. The low-resolution model tests indicate positive impact of the model forecasts. The higher resolution (T511) test for the period 22 Nov. - 14 Dec. 2000 indicated remarkable enhancements in the SH scores. The changes were introduced in operation starting from analysis cycle 00:00 on 9 April 2002.

References:

Abdalla, S. and L. Cavaleri, 2002. Effect of wind variability and variable air density on wave modeling, *Accepted for publication at Journal of Geophysical Research*.

Bauer, E., and R.Weisse, 2000. Determination of high-frequency wind variability from observations and application to North Atlantic wave modelling, *Journal of Geophysical Research*, **105**, pp. 26179-26190.

Bidlot, J., D.J. Holmes, P.A. Wittmann, R. Lalbeharry, and H.S. Chen, 2000. Intercomparison of the performance of the operational wave forecasting systems with buoy data, *Tech. Memo. 315*, E.C.M.W.F., 46pp.

Cavaleri, L. and G. Burgers, 1992. Wind gustiness and wave growth, *KNMI-Preprints*, 92-18, 38pp., Koninklijk Nederlands Meteorologisch Instituut, De Bilt, The Netherlands.

Cavaleri, L., L. Bertotti, M. Hortal, and M. Miller, 1997. Effect of reduced diffusion on surface wind and wave fields, *Monthly Weather Review*, **125**, pp.3024-3029.

Freilich, M.H., and D.B. Chelton, 1986. Wavenumber spectra of Pacific winds measured by the Seasat scatterometer, *Journal of Physical Oceanography*, **16**, pp.741-757.

Jacob, C., E. Andersson, A. Beljaars, R. Buizza, M. Fisher, E. Gerard, A. Ghelli, P. Janssen, G. Kelly, A.P. McNally, M. Miller, A. Simmons, J. Teixeira, and P. Viterbo, 2000. The IFS cycle CY21r4 made operational in October 1999, *ECMWF Newsletter*, No.87, pp.2-8.

Janssen, P.A.E.M., 1986. On the effect of gustiness on wave growth, *KNMI Afdeling Oceanografisch Onderzoek memo 00-86-18*, 17pp., Koninklijk Nederlands Meteorologisch Instituut, De Bilt, The Netherlands.

- Komen, G.J., L. Cavaleri, M. Donelan, K. Hasselmann, S. Hasselmann and P.A.E.M. Janssen, 1994. *Dynamics and Modelling of Ocean Waves*, 532pp., Cambridge University Press, Cambridge, UK.
- Miles, J. and G. Ierley, 1998. Surface-wave generation by gusty wind, *Journal of Fluid Mechanics*, **357**, pp.21-28.
- Munn, R.E., 1966. *Descriptive Micrometeorology*, 245pp., Academic Press, N.Y.
- Panofsky, H.A., H. Tennekes, D.H. Lenschow and J.C. Wyngaard, 1977. The characteristics of Turbulent velocity components in the surface layer under convective conditions, *Boundary-Layer Meteorology*, **11**, pp.355-361.
- Simmons, A., 1991. Development of the operational 31-level T213 version of the ECMWF forecast model, *ECMWF Newsletter*, No.56, pp.3-13.
- Smith, S.D., K.B. Kataros, W.A. Oost and P.G. Mestager, 1990. Two major experiments in the humidity exchange over the sea (HEXOS) program, *Bulletin of the American Meteorological Society*, **71**, pp.161-172.
- Tournadre, J., and S. Blanquet, 1994. Wind speed and wave mesoscale variability from *in situ* and altimeter data, *The Global Atmosphere and Ocean System*, **2**, pp.221-245.

2. Treatment of Spurious Charnock Parameter:

Wave Adjustment at the Sea Ice Boundary:

The sea ice mask used when producing the initial wave field from any given run may sometime be different than the sea ice mask used by the run itself. For example, a coupled forecast run starts from analysis wave fields which were obtained with a forecast sea ice fraction field whereas the forecast run uses the analysed sea ice fraction. In such a case, there are points along the sea ice boundary that are now considered sea points but for which no initial wave field is available (beside the usual noise level). In some instances, when the local wind is not small, the induced surface stress, and therefore the feedback Charnock parameter is abnormally high since waves have to be created in the grid-box from a calm sea. In order to reduce the impact of such points, an initial wave field is generated for those points based on the local wind and the fetch limited JONSWAP parametric laws.

Numerical Spurious Charnock:

When determining the wave stress or the drag coefficient, small numbers were added to the square of both U_{10} and u^* to prevent numerical overflow. The added numbers are sometimes of the same order of magnitude than the actual values. Instead of adding a small number, the maximum of the actual value and a rather smaller number should be taken. This procedure reduces the number of spurious cases with very high Charnock parameter.

These two changes have resulted in smoother Charnock field as attested by the behaviour of the norms for a 10-day forecast run (Figure 4).

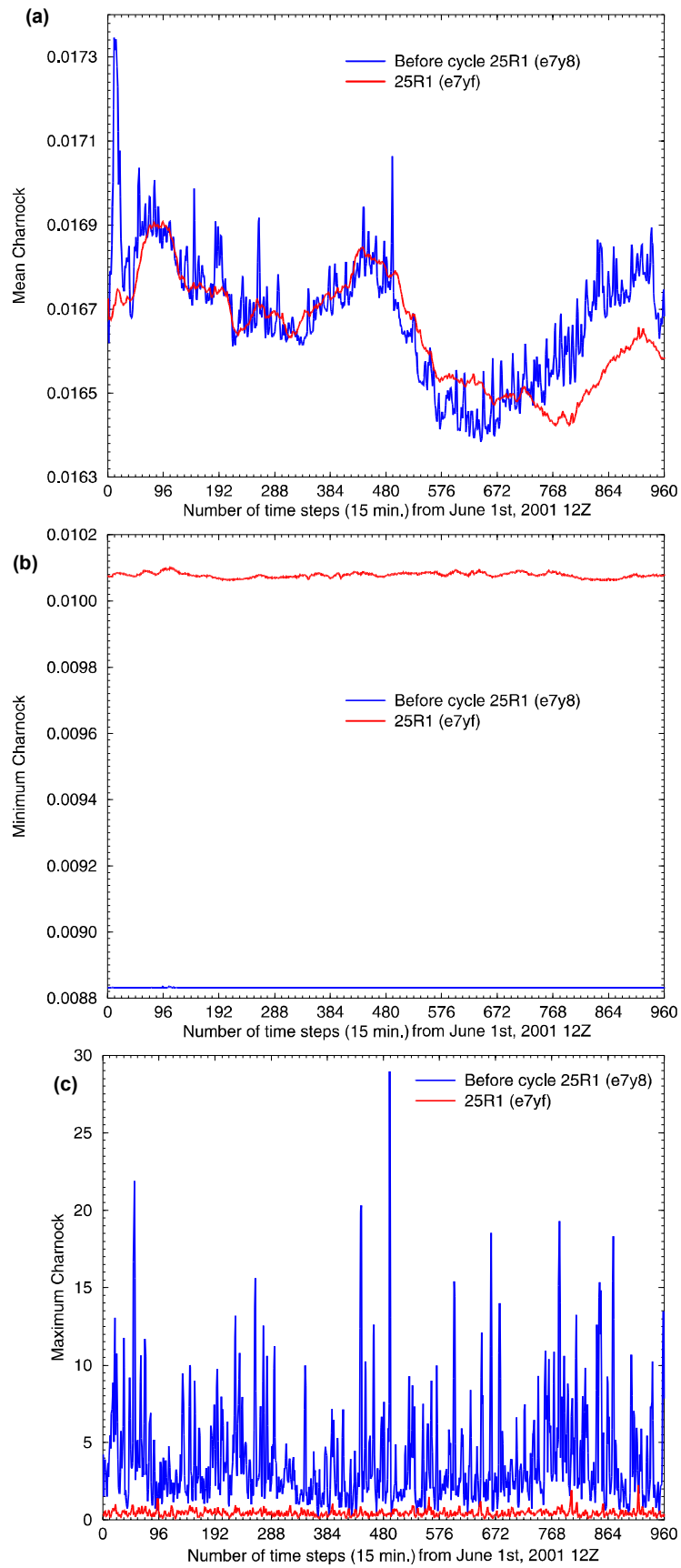


Figure 4: Evolution of the mean (a), minimum (b) and maximum (c) of the Charnock parameter for a 10-day forecast before the change to numerical relation used to determine the wave stress and the drag coefficient and since then.

3. Data Analysis:

Blacklisting:

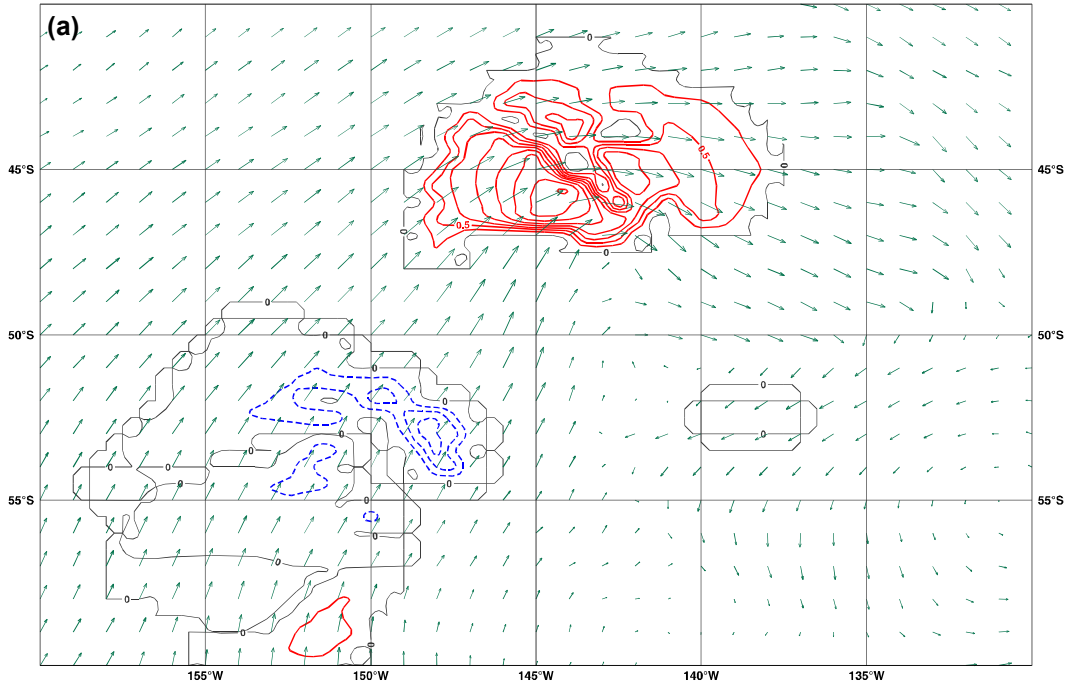
A blacklisting procedure has been implemented for the wave observations assimilated by WAM. It is a separate list than that of the atmospheric model. For the time being, the blacklist file is available for all computers with the name \$XDATA/wave/blackwave. The blacklist file is self-explanatory and only requires the knowledge of the BUFR codes for the satellite identifier, the sensor identifier and the parameter(s) to be blacklisted. The parameter(s) in question will then be blacklisted for a specified period of time, over a specified area (it could be global) and for a specified range of values.

Other Issues:

The update to the friction velocity (u_*) following the assimilation of altimeter data in windsea situations is now based on the simple windsea recognition scheme similar to the scheme used in the post-processing of windsea. It was found that the old windsea scheme had the tendency to leave out certain grid points (Figure 5a) resulting in non-smooth wind speed increments. The new scheme fares much better (Figure 5b). The threshold used in determining the windsea duration has been lowered to windsea wave height of 0.04 m instead of the old value of 0.40 m. It was found that under relatively low wave height conditions, this threshold would prevent any windsea spectral update at few grid points and results in analysis increments with holes as can be seen in Figure 6a. Lowering that threshold solved that problem as can be seen in Figure 6b. Finally, a call to the wind input source term is performed after the update to u_* to insure that the induced wave stress is in better balanced with the u_* update. All changes resulted in smoother wind speed increments.

There is an extra consistency check on the spectral updates following the altimeter wave height assimilation based on the wave height analysis increments. Very low frequency spectral updates are no longer allowed.

ECMWF Analysis VT: Saturday 2 December 2000 18UTC Surface: 10 mtr u/10 mtr v
 ECMWF Analysis VT: Saturday 2 December 2000 18UTC 10m **wind speed modified by wave model
 Wave parameter 245 analysis minus first guess (e5s2)



ECMWF Analysis VT: Saturday 2 December 2000 18UTC Surface: 10 mtr u/10 mtr v
 ECMWF Analysis VT: Saturday 2 December 2000 18UTC 10m **wind speed modified by wave model
 Wave parameter 245 analysis minus first guess (e6n6)

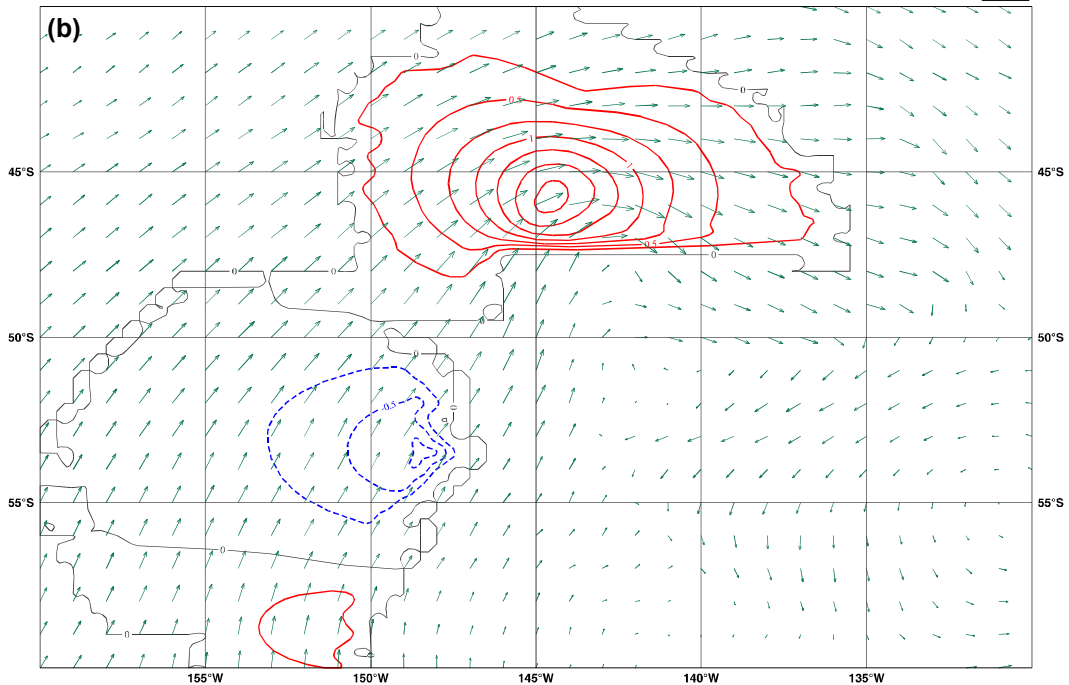
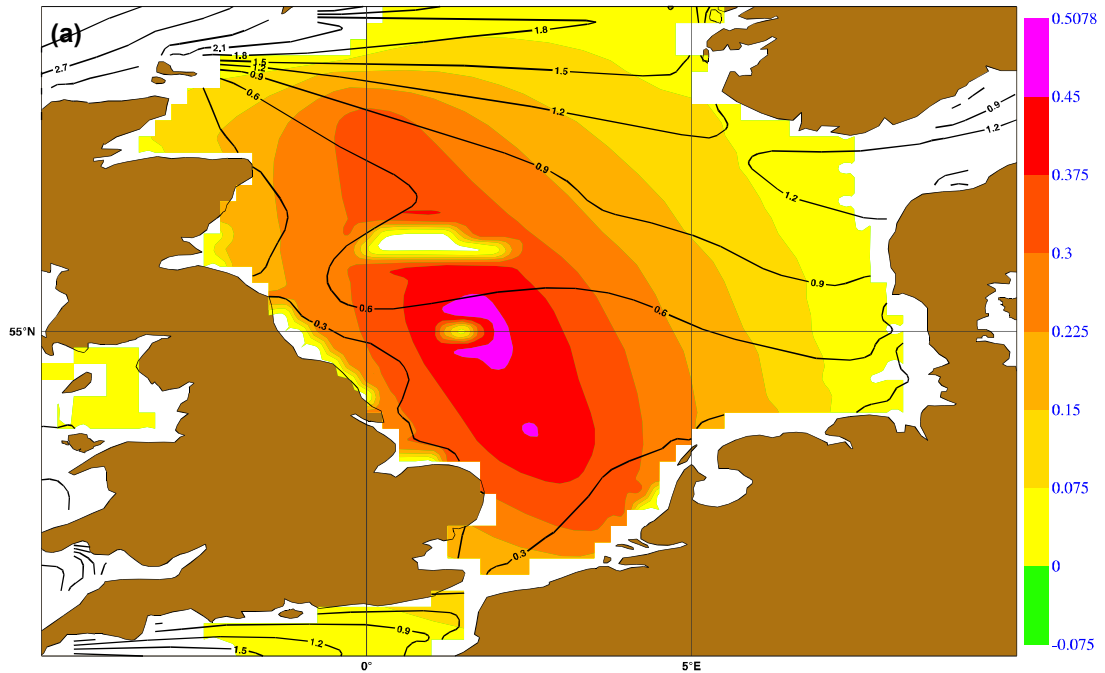


Figure 5: Contours of the wind speed analysis increments as derived from the altimeter wave height assimilation for a typical area with dominant windsea: (a) before CY25R1 where the windsea detection scheme did not always yield windsea at grid points where it should have; (b) since CY25R1 with the more robust scheme. The analysis wind field used to force WAM is displayed as vectors.

ECMWF Analysis VT:Wednesday 9 January 2002 00UTC Surface: **significant wave height
Wave parameter 229 analysis minus first guess (1)



ECMWF Analysis VT:Wednesday 9 January 2002 00UTC Surface: **significant wave height
Wave parameter 229 analysis minus first guess (e886)

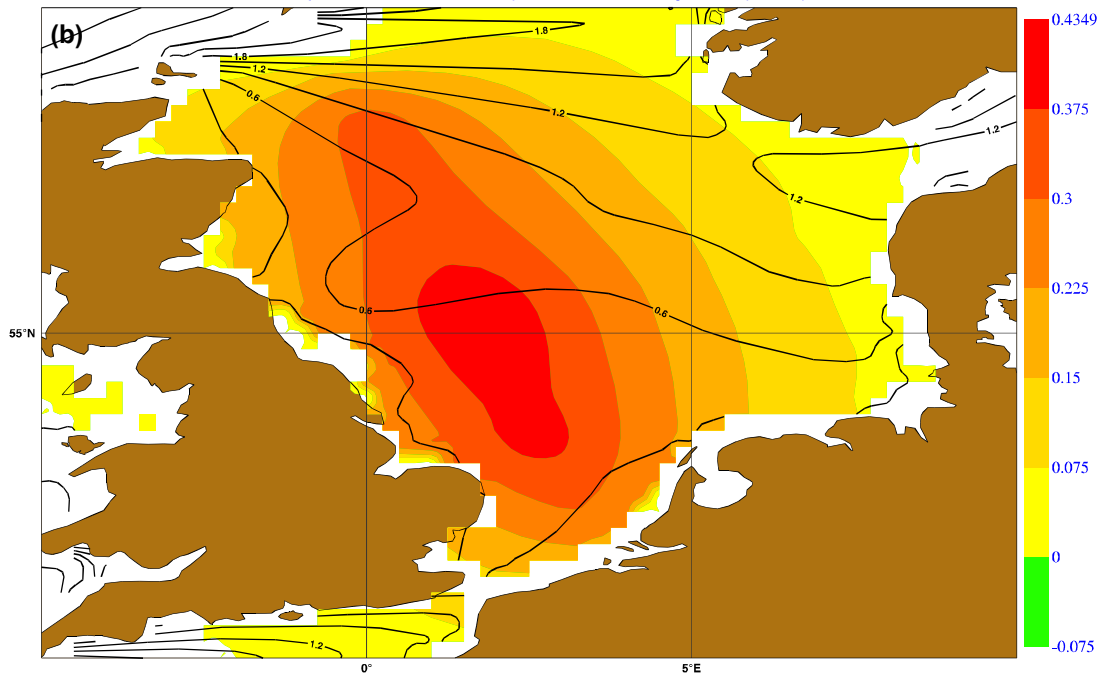


Figure 6: Colour shading of the wave height analysis increment derived from the altimeter wave height assimilation over a typical area with dominant small-amplitude windsea: (a) before CY25R1 when an artificially too high threshold prevented the spectral update at few grid points; (b) since CY25R1 with a much lower threshold. The first guess wave height is shown as contour lines.